Hybrid SNCR-SCR Technologies for NO_x Control: Modeling and Experiment

Jost O. L. Wendt
Dept. of Chemical and Environmental Engineering, University of Arizona, Tucson, AZ 85721

William P. Linak, Paul W. Groff, and Ravi K. Srivastava
Air Pollution Prevention and Control Division, MD-65, National Risk Management Research Laboratory, U.S. Environmental Protection Agency, Research Triangle Park, NC 27711

The hybrid process of homogeneous gas-phase selective noncatalytic reduction (SNCR) followed by selective catalytic reduction (SCR) of nitric oxide (NO) was investigated through experimentation and modeling. Measurements, using NO-doped flue gas from a gas-fired 29 kW test combustor, provided data that allowed a fundamentally based catalyst monolith model, adapted from the literature, to be calibrated. The SCR model, which included pore and gas film diffusion (molecular and Knudsen) and Langmuir-Hinshelwood surface reaction kinetics, used published values for the catalyst preexponential factor and activation energy, and experimental measurements to determine the previously unavailable ammonia (NH_3) adsorption coefficient on the catalyst surface. Then, with no further adjustment, a combined SNCR-SCR model was developed using literature values for the reaction rate coefficients of 112 elementary homogeneous reactions. This combined model agreed well with combined SNCR-SCR data. The combined model was then extrapolated to practical coal combustion conditions, and the economic benefits of a combined SNCR-SCR process were explored. With a desired total NO reduction of 95% and NH_3 slip in the exhaust constrained not to exceed 5 ppm, adding SNCR led to only modest decreases in the required SCR catalyst volume. Estimated system capital and annualized costs were not economically viable unless the SNCR portion by itself reduced more than 60% of the NO.

Introduction

Hybrid SNCR-SCR technologies, as applied for nitric oxide (NO) control from stationary combustion systems, combine selective noncatalytic reduction (SNCR) and selective catalytic reduction (SCR) with the intention of optimizing performance (NO reduction) and minimizing cost (Gullett et al., 1994; Fujino et al., 1995; Wallace et al., 1995; Urbas and Boyle, 1997; Groff and Gullett, 1997). SCR is highly effective, but involves relatively high capital expense (Urbas and Boyle, 1997; NESCAUM, 1998). SNCR is less effective under practical field conditions because of inhomogeneities caused by incomplete mixing (Stamey-Hall and Neuffer, 1994; Jones et al., 1995; Hunt et al., 1997), but involves less capital expense and similar operating expenses. By combining these technologies, it is hypothesized that SCR capital costs might be reduced with NO reduction levels beyond those achievable by SNCR alone. Both processes involve the use of nitrogen-based reducing agents, which react with NO to produce diatomic nitrogen (N_2) and water. SNCR involves the addition of urea [$CO(NH_2)_2$], ammonia (NH_3), or cyanuric acid [$(HOCN)_3$], and homogeneous reaction with NO at appropriate flue-gas temperatures. For full-scale applications, NO reductions of approximately 30 to 60% have been achieved (ICAC, 1994a; Himes et al., 1995), even though bench-scale testing often achieves greater reductions (Miller and Bowman, 1989). Process concerns include temperature windows, temperature variability, adequate mixing, reagent oxidation, and NH_3 slip. SCR, which utilizes NH_3 as the reducing agent and heterogeneous reaction of NO on a catalyst, can achieve reductions

Correspondence concerning this article should be addressed to W. P. Linak.

greater than 95% (Fujino et al., 1995). Practical implementation of SCR on coal-fired combustion sources, however, limits its NH_3 slip to 2 to 5 ppm, to prevent balance-of-plant impacts and to ensure that fly ash marketability is not affected. SCR performance (and capital cost) is directly related to the catalyst volume and associated space velocity. By using SNCR to accomplish a sizable portion of the NO reduction, it is anticipated that the SCR catalyst volume (and system costs) can be reduced while maintaining comparable NO reductions compared to SCR alone. Additionally, a common SNCR problem related to high NH_3 slip can be mitigated (and utilized) by the SCR catalyst.

In order to determine conditions under which hybrid SNCR-SCR processes are economically viable in practice, it is necessary first to develop an accurate, validated model of the combined process. The research described here presents such a model, its validation on a natural gas-fired combustor in the laboratory, and its subsequent application to an economic analysis of hybrid SNCR-SCR processes applied to coal-fired boilers in the field.

Selective noncatalytic reduction

Homogeneous SNCR of NO occurs in flue gases when a nitrogenous species such as NH_3 (Thermal De-NO_x process), urea (NOXOUT process), or cyanuric acid (RAPRENOX process), is injected into flue gas, with each reagent injected at its own optimum temperature. In the research presented here, the experimental efforts focused solely on NO reduction by NH_3. However, the modeling efforts validated the experimental results using NH_3 and also examined the use of urea because of its common use as an SNCR reagent for utility applications. As discussed below, the homogeneous mechanisms and rate constants associated with these SNCR reagents are well documented. No attempt is made here to model SNCR processes involving cyanuric acid.

Thermal De-NO_x has its origins in the observation that NH_3 would selectively react with NO under appropriate temperatures to yield N_2 (Lyon, 1975). The process works because the mechanism by which NO is reduced has a significant chain-branching component and, under the proper conditions, this chain branching produces a pool of radical species that allow the overall mechanism to be self-sustaining. Miller and Bowman (1989) present a detailed review of the process and associated rate constants, and identify the following reactions to be important

$$NH_3 + OH \Leftrightarrow NH_2 + H_2O \quad (1)$$

$$NH_3 + O \Leftrightarrow NH_2 + OH \quad (2)$$

$$NH_2 + NO \Leftrightarrow N_2 + H_2O \quad (3)$$

$$NH_2 + NO \Leftrightarrow NNH + OH \quad (4)$$

$$NNH + NO \Leftrightarrow N_2 + HNO \quad (5)$$

$$HNO + M \Leftrightarrow H + NO + M \quad (6)$$

$$H + O_2 \Leftrightarrow OH + O. \quad (7)$$

First, NH_2 is produced by the reaction of NH_3 with OH (Reaction 1) and to a lesser extent with O (Reaction 2). NH_2 then reacts with and reduces NO via Reactions 3 and 4. However, in order to be self-sustaining, the $NH_2 + NO$ reaction must directly or indirectly regenerate OH and O to continue the NH_3 to NH_2 conversion. This regeneration is accomplished via Reactions 4–7. Reaction 6 is a three-body reaction, with M representing any species.

Ammonia can be introduced as a gas or an aqueous solution. However, NH_3 is toxic and can be difficult to handle. As a result, alternate agents and processes have been developed to improve reagent handling and NO removal performance. These agents include urea (Arand et al., 1980) and cyanuric acid (Perry and Siebers, 1986; Perry, 1988). Once introduced, urea and cyanuric acid undergo thermal decomposition to yield $NH_3 + HNCO$ (Muzio et al., 1990; Braun et al., 1991; Caton and Siebers, 1989) and HNCO, respectively (Miller and Bowman, 1989). NH_3 reduces NO via Reactions 1–7. However, once released into the gas phase, the HNCO reacts primarily according to the mechanism (Miller and Bowman, 1989; Lyon and Cole, 1990)

$$HNCO + OH \Leftrightarrow NCO + H_2O \quad (8)$$

$$NCO + NO \Leftrightarrow N_2O + CO \quad (9)$$

$$HNCO + H \Leftrightarrow NH_2 + CO. \quad (10)$$

An important difference between NH_3 and urea or cyanuric acid is that both urea and cyanuric acid reagents generate HNCO, NCO, and N_2O as major products of reaction, while NH_3 does not (Siebers and Caton, 1990). Thus, both urea and cyanuric acid generate substantially more N_2O emissions when used as SNCR reagents. In fact, measurements indicate that, typically, less than 5% of the NO reduced is converted to N_2O when NH_3 is used. This compares to conversions greater than 10% for urea. Comparison of urea and cyanuric acid as SNCR reagents shows that urea generates less N_2O under equivalent conditions (De Soete, 1990a,b; Muzio et al., 1990; Kramlich and Linak, 1994). This is significant because anthropogenic N_2O emissions have been shown to contribute to stratospheric ozone destruction and have been implicated in possible increases in global temperatures.

Miller and Bowman (1989) indicate that a major limitation of SNCR is that it occurs only within a narrow temperature window, between approximately 1,150 and 1,350 K. In large-scale facilities, incomplete mixing often limits the NO reduction even at optimum temperatures. Thus, considerable research efforts have focused on methods to promote and enhance performance. Many of these approaches involve reagent injection techniques that enhance mixing and the co-injection of combustible promoting agents such as CO, H_2, and CH_4 (Chen et al., 1989; Teixeira et al., 1992; Caton and Siebers, 1991). In general, the promoting agents have the effect of shifting and/or broadening the optimum temperature window. The temperature shifts because the oxidation of the combustible promoter generates excess free radicals that are needed to initiate the reaction of the SNCR reagent.

In full-scale utility boiler applications, it is difficult to ensure that all the injected NH_3 or urea additive is subjected to the optimum temperature window for homogeneous NO destruction. In this work, this practical difficulty was simulated by modeling SNCR at "effective temperatures" that were both

higher and lower than the optimum temperature, since a detailed mathematical description of an imperfect turbulent mixing process coupled with chemical reaction was outside the scope of this work.

Selective catalytic reduction

SCR refers to the heterogeneous reduction of NO by added NH_3 over a catalyst. The process is, at present, applied only to stationary sources of NO, with mobile sources being dominated by direct catalytic reduction without use of a reagent such as NH_3. SCR is presently being applied to utility and industrial systems in Japan and Germany, and is coming into increasing use in other parts of the world including the U.S.

Most SCR systems are based on catalysts composed of either noble metal or vanadium active components deposited on metal plates or incorporated within ceramic substrates. Meier and Gut (1978) examined the kinetics over a platinum catalyst using a Langmuir-Hinshelwood rate expression. Beeckman and Hegedus (1991) examined the design and kinetics associated with a vanadium-titanium monolith (similar to the type investigated here) in which the vanadium catalyst is deposited on porous anatase-type titanium and extruded into the shape of square-channeled monoliths. The overall chemical reaction has the stoichiometry

$$4NO + 4NH_3 + O_2 \Leftrightarrow 4N_2 + 6H_2O. \qquad (11)$$

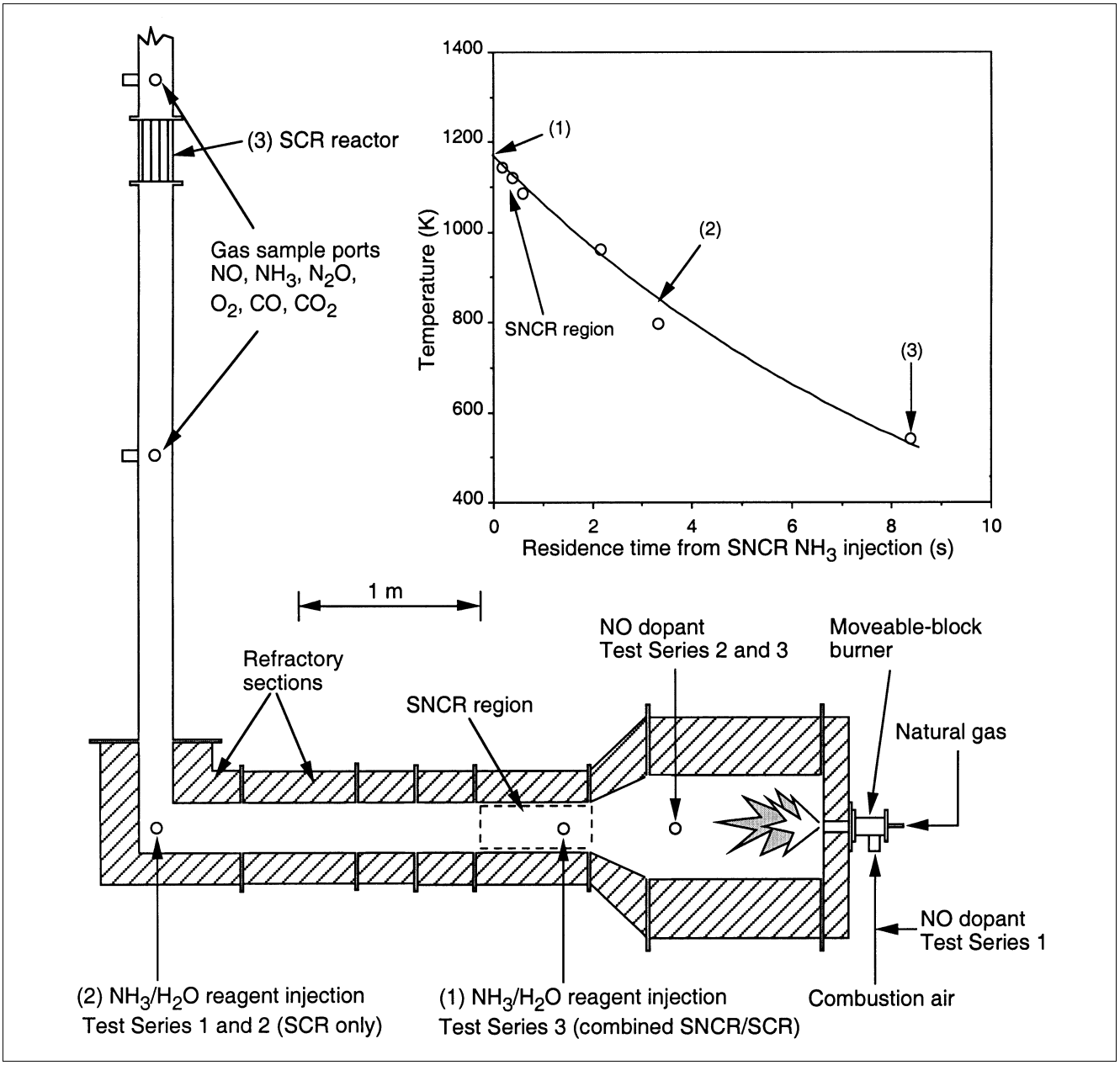

Figure 1. EPA horizontal-tunnel combustor and experimental temperature profile.

This equation is equimolar with respect to both NO and NH_3 which is an important point in the model described below. For vanadium-titanium catalysts, Beeckman and Hegedus (1991) also propose that the intrinsic reaction rate can be based on a Langmuir-Hinshelwood type rate expression

$$R_{NO} = k_0 \exp(-E/RT)\, C_{NO} \left[K_{NH_3} C_{NH_3} / \left(1 + K_{NH_3} C_{NH_3}\right) \right] \quad (12)$$

where R_{NO}, k_0, E, R, T, C_{NO}, C_{NH_3}, and K_{NH_3} are the intrinsic NO reaction rate, pre-exponential factor, activation energy, gas constant, absolute temperature, NO and NH_3 concentrations, and NH_3 adsorption constant, respectively. Beeckman and Hegedus (1991) were able to obtain values for k_0 and E, but *not* K_{NH_3}, although they acknowledged possible inaccuracies in their value for E.

Approach

The objective of the research presented here was to build and expand upon the literature contributions of others in order to investigate the implementation of combined SNCR-SCR systems for NO control. The approach was organized as follows:

Experiments. Separate SCR-only and combined SNCR-SCR experiments were conducted using a natural-gas-fired

Table 1. Reactor and Flue-Gas Parameters

	SCR model Notation	Experimental Combustor	Full-Scale Coal Combustor*
Reactor Parameters			
Reactor width†		1.5e-1 m (15.0 cm)	
Reactor depth†		1.05e-1 m (10.5 cm)	
Reactor length†	L	3.56e-1 m (35.6 cm)	
Reactor volume	V	5.607e-3 m^3 (5,607.0 cm^3)	
Reactor (catalyst) mass†		3.0976 kg (3,097.6 g)	
Reactor bulk density		5.5e + 2 kg/m^3 (0.55 g/cm^3)	
Cell width†	c_w	3.2e-3 m (0.32 cm)	7.4e-3 m (0.74 cm)
Cell depth†	c_d	3.2e-3 m (0.32 cm)	7.4e-3 m (0.74 cm)
Cell shape factor	B	2.976 (for squares)	2.976 (for squares)
Hydraulic radius	R_h	1.6e-3 m (0.16 cm)	3.7e-3 m (0.37 cm)
Wall thickness†	W	5.5e-4 m (0.055 cm)	1.2e-3 m (0.12 cm)
Number of cells†		1120	4,936
Open gas flow area		1.147e-2 m^3 (114.7 cm^2)	2.703e-1 m^2 (2,703 cm^2)
Reactor cross-sectional area		1.575e-2 m^2 (157.5 cm^2)	3.650e-1 m^2 (3650 cm^2)
External film area per unit length		1.434e + 1 m^2/m (1.434e + 3 cm^2/cm)	1.461e + 2 m^2/m (1.461e + 4 cm^2/cm)
Film area per reactor volume	A_e	9.102e + 2 m^2/m^3 (9.102 cm^2/cm^3)	4.002e + 2 m^2/m^3 (4.002 cm^2/cm^3)
Catalyst BET surface area †		7.704e + 4 m^2/kg (77.04 m^2/g)	7.704e + 4 m^2/kg (77.04 m^2/g)
Catalyst density	ρ_{cat}	1.89e + 3 kg/m^3 (1.89 g/cm^3)	1.89e + 3 kg/m^3 (1.89 g/cm^3)
Catalyst pore specific vol. †		2.59e-4 m^3/kg (0.259 cm^3/g)	2.59e-4 m^3/kg (0.259 cm^3/g)
Catalyst average pore dia.†		1.34e-8 m (1.34e-6 cm)	1.34e-8 m (1.34e-6 cm)
Catalyst porosity	ϵ	0.49	0.49
Catalyst specific surface area	S_v	7.704e + 6 m^2/m^3 (7.704e + 4 cm^2/cm^3)	7.704e + 6 m^2/m^3 (7.704e + 4 cm^2/cm^3)
Gas Parameters			
Gas flow		9.257e-3 Nm^3/s (9.257e + 3 Ncm^3/s)	1.0 Nm^3/s (1.0e + 6 Ncm^3/s)
Gas temp. (@ SCR reactor)	T	523 K	672 K
Actual gas flow	F	1.773e-2 m^3/s (1.773e + 4 cm^3/s)	2.462 m^3/s (2.462e + 6 cm^3/s)
Gas velocity	v_g	1.546 m/s (154.6 cm/s)	9.108 m/s (910.8 cm/s)
Space velocity		3.163/s	
Gas viscosity	μ	2.77e-5 kg/m·s (2.77e-4 g/cm·s)	3.26e-5 kg/m·s [3.26e-4 g/cm·s]
Gas density	ρ	6.75e-1 kg/m^3 (6.75e-4 g/cm^3)	5.21e-1 kg/m^3 (5.21e-4 g/cm^3)
Reynolds number	Re	120.7	1076
NO molecular diffusion coeff.	D_{NO}	5.423e-5 m^2/s (0.5423 cm^2/s)	7.898e-5 m^2/s (0.7898 cm^2/s)
NH_3 molecular diffusion coeff.	D_{NH_3}	8.603e-5 m^2/s (0.8603 cm^2/s)	1.253e-4 m^2/s (1.253 cm^2/s)
NO Knudsen diffusion coeff.	$D_{Kn,NO}$	5.426e-6 m^2/s (0.05426 cm^2/s)	6.151e-6 m^2/s (0.06151 cm^2/s)
NH_3 Knudsen diffusion coeff.	D_{Kn,NH_3}	7.203e-6 m^2/s (0.07203 cm^2/s)	8.165e-6 m^2/s (0.08165 cm^2/s)
NO effective diffusion coeff.	$D_{e,NO}$	1.182e-6 m^2/s (0.01182 cm^2/s)	1.368e-6 m^2/s (0.01368 cm^2/s)
NH_3 effective diffusion coeff.	D_{e,NH_3}	1.593e-6 m^2/s (0.01593 cm^2/s)	1.837e-6 m^2/s (0.01837 cm^2/s)
NO external mass transfer coeff.	km_{NO}	5.217e-2 m/s (5.217 cm/s)	3.223e-2 m/s (3.223 cm/s)
NH_3 external mass transfer coeff.	km_{NH_3}	8.176e-2 m/s (8.176 cm/s)	5.086e-2 m/s (5.086 cm/s)

*Basis is 1 Nm^3/s of flue gas at 3.7 Nm/s. Catalyst cell dimensions and wall thickness for coal applications provided by Rummenhohl (1999).
†Reactor parameters measured *a priori* for the experimental combustor only.

combustor operated at 29 kW. These experiments involved integral reactor measurements over a wide range of initial NO and NH_3 concentrations, but only within a narrow range of SCR temperatures from 500 to 550 K.

SCR Model Development. An SCR model was developed for the actual catalyst monolith used in the experiment. This model was based on the approach of Beeckman and Hegedus (1991), with physical catalyst parameters determined for the actual catalyst used here. Also, because of differences in the range of applicable concentrations of NH_3, the SCR model required a different numerical method of solution. This model was fitted to the SCR-only data to extract the missing parameter K_{NH_3} (using Beeckman and Hegedus's values for k_0 and E) or alternatively, to extract either two or all three parameters (k_0, E, and K_{NH_3}).

SNCR and Combined SNCR-SCR Models. A CHEMKIN (Kee et al., 1992)-based SNCR model, using a modified Miller and Bowman (1989) mechanism with 112 reactions and 32 species, was developed and combined with the SCR model. Data from the combined SNCR-SCR experiments were then compared to predictions of the combined model with no further adjustment of parameters.

Predictions and Model Extrapolation to Coal Combustion. The validated SNCR-SCR model was then used to extrapolate to full-scale coal combustion systems with different catalyst geometric properties, but identical intrinsic kinetic properties. This field model, in which a key constraint is a limitation of 5 ppm NH_3 slip leaving the SCR reactor, was then used to develop design tools to predict performance and potential economic benefits of combined SNCR-SCR operation.

Each of these steps is now described in detail.

Experiments

Laboratory swirl flame combustor

Experiments were performed using the laboratory-scale horizontal-tunnel combustor rated at 82 kW and illustrated

Table 2. NO, NH_3, and N_2O Measurements*

Test No.	Pre-SNCR NO (ppm)	Pre-SNCR NH_3 (ppm)†	SNCR λ	Pre-SCR NO (ppm)	Pre-SCR NH_3 (ppm)	SCR λ	SCR Temp (K)	Post-SCR NO (ppm)	Post-SCR NH_3 (ppm)	Post-SCR N_2O (ppm)
SCR-Only Experiments										
1-2/25A				142.1	43.3	0.30	546	91.2	6.2	—
1-2/25B				164.3	117.6	0.72	546	75.4	7.6	—
1-2/25C				185.0	201.2	1.09	545	61.7	8.1	—
1-2/26A				131.5	18.5	0.14	516	107.1	8.3	—
1-2/26B				131.0	41.9	0.32	517	98.7	7.5	—
1-2/26C				132.2	61.5	0.47	518	88.7	9.4	—
1-2/26D				131.6	91.2	0.69	518	70.7	9.0	—
1-2/26E				132.9	118.7	0.89	518	55.1	9.5	—
2-4/8A				144.3	3.0	0.02	506	120.7	2.8	0.2
2-4/8B				148.1	95.0	0.64	501	111.7	3.2	0.3
2-4/8C				146.7	113.5	0.77	501	100.7	4.2	0.3
2-4/8D				149.8	147.3	0.98	502	89.2	4.8	0.4
2-4/8E				153.9	242.3	1.57	503	61.8	3.8	0.6
2-4/9A				436.3	110.9	0.25	502	367.6	3.0	0.5
2-4/9B				489.3	317.0	1.15	507	297.7	4.8	1.0
2-4/9C				479.5	396.9	1.45	508	222.1	5.6	0.0
2-4/14A				827.5	213.8	0.26	540	608.1	1.7	0.0
2-4/14B				858.7	519.8	0.61	541	361.8	7.4	1.2
2-4/14C				914.5	620.7	0.68	542	291.1	5.0	1.5
2-4/14D				908.4	674.2	0.87	541	205.9	16.7	1.7
2-4/21A				768.5	210.8	0.27	501	650.6	1.7	0.0
2-4/21B				705.3	520.2	0.74	497	454.0	3.5	1.1
2-4/21C				727.2	614.5	0.85	499	292.3	15.6	1.3
2-4/21D				747.9	687.4	0.92	501	237.6	53.2	0.0
2-4/21E				710.8	912.3	1.28	497	228.1	375.0	4.1
2-5/12A				417.1	78.3	0.19	516	393.4	2.1	0.5
2-5/12B				354.9	278.4	0.78	506	261.6	2.7	2.6
2-5/12C				357.0	345.0	0.97	505	204.7	3.7	2.7
2-5/12D				370.0	367.9	0.99	505	131.6	18.4	2.3
2-5/12E				363	575.5	1.58	506	107.3	—	—
Combined SNCR/SCR Experiments										
3-4/10A	127.2	34.6	0.27	106.1	1.9	0.02	551	96.7	1.5	0.0
3-4/10B	127.8	56.4	0.44	82.2	2.6	0.03	550	76.6	2.3	0.0
3-4/10C	131.6	73.3	0.56	78.7	3.6	0.05	550	69.0	2.2	0.0
3-4/10D	138.8	78.4	0.56	80.6	9.7	0.12	549	67.9	2.5	2.8
3-4/10E	141.1	141.4	1.00	69.4	37.7	0.54	548	47.9	2.3	4.9

*All concentrations on wet basis.
†Pre-SNCR NH_3 was calculated based on measured system flow rates.

in Figure 1. This refractory-lined research combustor was designed to simulate the time/temperature and mixing characteristics of practical combustion systems. Natural gas and combustion air were introduced through an International Flame Research Foundation (IFRF) movable-block variable-air-swirl burner. Swirling air passed through the annulus around the fuel injector promoting flame stability and attachment on the refractory quarl (high swirl, IFRF type 2 flame). NO dopant was added (see Figure 1) to vary the NO concentrations from approximately 125 to 1,000 ppm. Axial ports permitted detailed temperature measurement, addition of NH_3 reagent, and gas sampling before and after the SCR catalyst. Further details regarding the experimental combustor can be found elsewhere (Linak et al., 1994).

Preliminary axial temperature measurements were taken to identify appropriate locations for the NH_3 reagent injection and SCR catalyst. It was found that a reduced furnace load of 29 kW produced a temperature profile with suitable SNCR ($\sim$1,150–1,350 K) (Miller and Bowman, 1989) and SCR ($\sim$533 K) locations, as indicated in Figure 1.

Ammonia reagent and SCR catalyst

Reagent solutions were prepared in-house using commercially available strong NH_3 solutions (29.5 wt. % NH_3) and distilled water. Multiple solutions of varying concentration were prepared to allow constant reagent feed rate ($\sim 1.67 \times 10^{-7}$ m^3/s, 10 mL/min) for all values of NH_3/NO stoichiometry (λ) examined, so as not to alter temperature distributions between the different conditions examined. Reagent solutions were atomized along the combustor centerline using 7.67×10^{-4} m^3/s (46 NL/min) of air. A vanadium-titanium catalyst monolith, similar to the type used by Beeckman and Hegedus (1991), was mounted at the stack location indicated as [(3) SCR reactor] in Figure 1. Catalyst parameters listed in Table 1 were determined or calculated based on direct measurements performed in-house.

Gas sampling and analysis

Flue-gas composition was monitored for nitrogenous species NO, NH_3, and N_2O, as well as O_2, CO, and CO_2 at locations before and after the SCR catalyst (see Figure 1). Extractive samples were conditioned (filtered and dried) and directed to continuous NO (chemiluminescence), O_2 (paramagnetic), and CO and CO_2 (nondispersive infrared) analyzers. Conditioned samples were also directed to an on-line gas chromatograph/electron capture detector N_2O analysis system. This automated batch analysis provided N_2O measurements approximately every 480 s (8 min) (Ryan and Linak, 1992; Kramlich and Linak, 1994). Filtered, heated samples were also directed for continuous NH_3 (nondispersive infrared) analysis. By appropriate use of valving, sampling could be quickly alternated between post-SNCR (pre-SCR) and post-SCR locations.

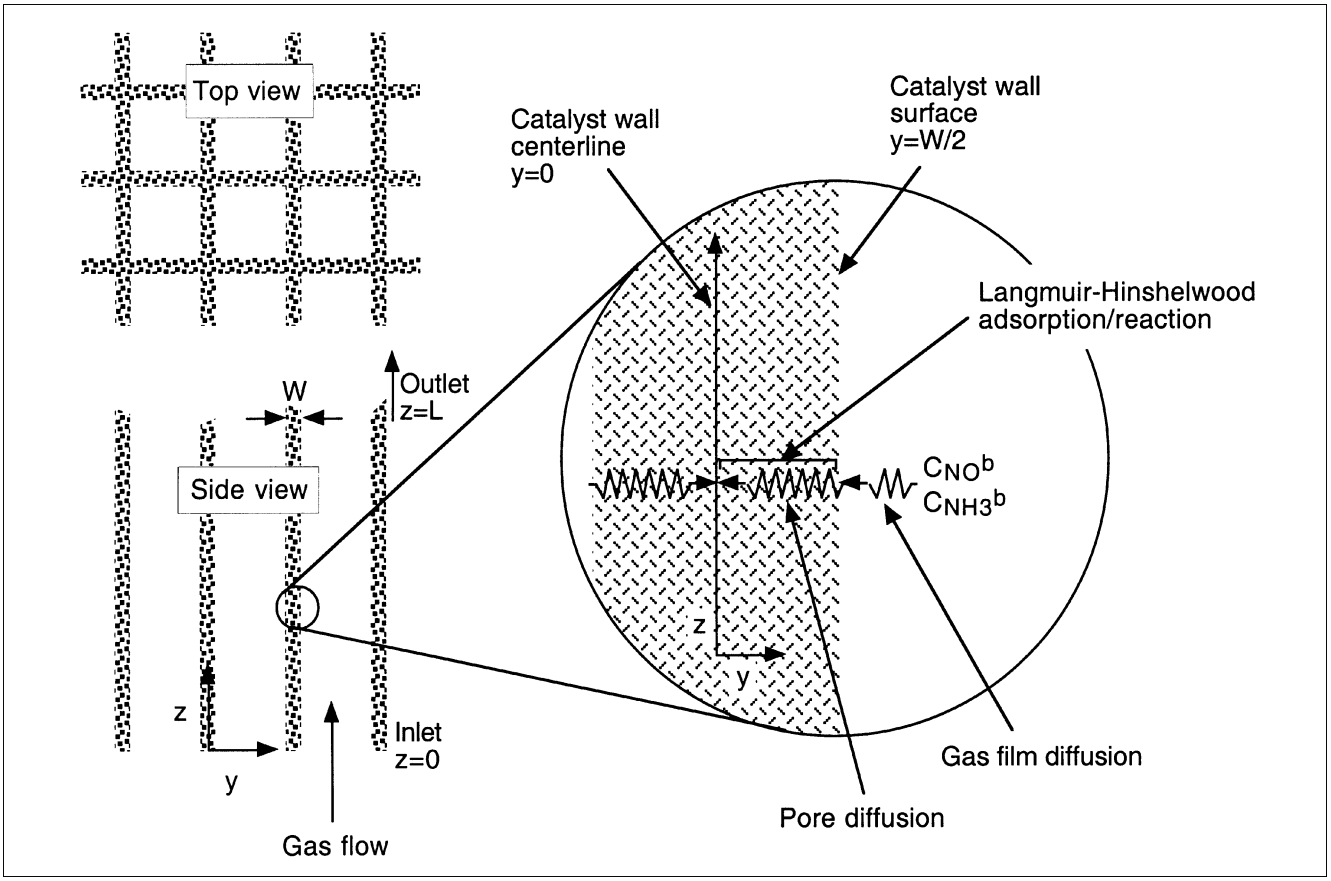

Figure 2. Geometry, mass transfer, and kinetic processes occurring within the catalyst monolith.

Table 2 summarizes NO, NH_3, and N_2O measurements for all the experimental conditions examined and used for model calibration. All concentrations are corrected to a wet basis. Three test series were performed. Test Series 1 includes eight SCR-only tests in which NO dopant was added with the combustion air. Apparent from these measurements is that the pre-SCR NO was insensitive to the amount of NO dopant added, and this was likely due to natural air staging occurring within the IFRF burner. Subsequently, Test Series 2 includes 22 SCR-only tests in which NO dopant was added downstream of the flame (see Figure 1). This arrangement allowed the pre-SCR NO to be varied. For both Test Series 1 and 2, the SCR NH_3 reagent was added at a location well downstream of any SNCR activity (see Figure 1). Test Series 3 included five combined SNCR-SCR tests where the NH_3 reagent was introduced within a temperature window of SNCR activity. Table 2 includes only combined SNCR-SCR tests in which no additional NO dopant was added. Additional tests were performed varying NO, but the NO was found to channel and was not well mixed with the combustion gases in the SNCR region. However, this lack of extensive combined SNCR-SCR data was not believed to be limiting as the SNCR portion of the model is based on an established approach using validated kinetic rate information.

Data quality analysis

Pre-SCR concentration gradient tests were performed to ensure even distribution of reactants across the catalyst. Radial concentrations were measured in 2.54×10^{-2} m (2.54 cm) increments across the 2.032×10^{-1} m (20.32 cm) duct (see Figure 1). NO and NH_3 concentrations were 78.1 ± 20 and 3.1 ± 0.4 ppm, respectively. Combustion consistency was determined by averaging the temperature O_2 and CO_2 measurements over the longest contiguous test condition of 1.62×10^4 s (4.5 h). Average values and standard deviations of these temperature, O_2, and CO_2 measurements are 517 ± 17 K, $4.7\pm0.6\%$, and $7.9\pm0.6\%$, respectively (wet basis, 16% water by volume). Pre-SCR base line NO concentrations for the lowest, middle, and highest NO concentrations were 142 ± 7.6, 473 ± 7.4, and $1{,}003\pm14.6$ ppm, respectively. NH_3 concentrations varied from test to test with a base line condition of no injected NH_3. Consequently, no corresponding NH_3 averages and standard deviations are available.

SCR Model Development

Consider the catalyst monolith system presented in Figure 2. Following the approach of Beeckman and Hegedus (1991), at any axial position z a material balance describing diffusion and reaction in a section of catalyst along the transverse coordinate y perpendicular to z yields

$$D_{e,\mathrm{NO}}\,d^2C_{\mathrm{NO}}/dy^2 = S_v R_{\mathrm{NO}} \tag{13}$$

and

$$D_{e,\mathrm{NH_3}}\,d^2C_{\mathrm{NH_3}}/dy^2 = S_v R_{\mathrm{NH_3}} \tag{14}$$

where $D_{e,i}$, C_i, and R_i are the effective diffusion coefficients (including Knudsen and molecular diffusion terms), concentrations, and reaction rates of NO and NH_3, and S_v is the catalyst-specific surface area in square centimeters per cubic centimeter. R_{NO} is given by Eq. 12, with $R_{\mathrm{NH_3}}$ equivalent to R_{NO}. Boundary conditions are

$$dC_{\mathrm{NO}}/dy = 0 \qquad \text{and}$$
$$dC_{\mathrm{NH_3}}/dy = 0 \qquad \text{at} \quad y = 0 \tag{15}$$

and

$$km_{\mathrm{NO}}\left(C_{\mathrm{NO}}{}^{b} - C_{\mathrm{NO}}{}^{s}\right) = D_{e,\mathrm{NO}}\left(dC_{\mathrm{NO}}/dy\right)^{s} \qquad \text{and}$$
$$km_{\mathrm{NH_3}}\left(C_{\mathrm{NH_3}}{}^{b} - C_{\mathrm{NH_3}}{}^{s}\right) = D_{\mathrm{e,NH_3}}\left(dC_{\mathrm{NH_3}}/dy\right)^{s} \text{ at} \quad y = W/2 \tag{16}$$

where km_i is the external mass-transfer coefficient for NO and NH_3, and superscripts b and s indicate bulk and surface concentrations, respectively. Whereas Beeckman and Hegedus (1991) used the reaction stoichiometry to calculate the NH_3 concentration in the pore by difference from the NO concentration profile, this approach failed over the entire range of NO and NH_3 concentrations investigated here. Hence, Eq. 14 was solved directly for the NH_3 concentration, and this, together with iteration (described below), never allowed negative NH_3 concentrations in the catalyst pore.

Assuming plug flow within the monolith channels, and uniform concentrations across the bulk gas phase, a material balance along the axial coordinate z yields

$$dC_{\mathrm{NO}}{}^{b}/dz = -\left(VA_e km_{\mathrm{NO}}/LF\right)\left(C_{\mathrm{NO}}{}^{b} - C_{\mathrm{NO}}{}^{s}\right) \tag{17}$$

and

$$dC_{\mathrm{NH_3}}{}^{b}/dz = -\left(VA_e km_{\mathrm{NH_3}}/LF\right)\left(C_{\mathrm{NH_3}}{}^{b} - C_{\mathrm{NH_3}}{}^{s}\right) \tag{18}$$

where V, A_e, L, and F are the reactor volume, monolith specific surface area, reactor axial length, and gas-flow rate, respectively. Boundary conditions are

$$C_{\mathrm{NO}}{}^{b} = C_{\mathrm{NO}}{}^{b0} \qquad \text{and}$$
$$C_{\mathrm{NH_3}}{}^{b} = C_{\mathrm{NH_3}}{}^{b0} \qquad \text{at} \qquad z = 0. \tag{19}$$

With R_{NO} (and $R_{\mathrm{NH_3}}$) given by Eq. 12, a numerical solution of Eqs. 13–19 allows the prediction of NO reduction across the SCR reactor and at any location within the catalyst.

Finally, the external mass-transfer coefficients for developing laminar flow in rectangular ducts are given by the Hawthorn correlation (Hegedus, 1973; Beeckman and Hegedus, 1991)

$$km_{\mathrm{NO}} = \left(D_{\mathrm{NO}}/2R_h\right)B\left[1 + 0.095\left(2R_h/L\right)ReSc_{\mathrm{NO}}\right]^{0.45} \tag{20}$$

and

$$km_{NH_3} = \left(D_{NH_3}/2R_h\right) B\left[1 + 0.095(2R_h/L)\, ReSc_{NH_3}\right]^{0.45} \tag{21}$$

where R_h, Re, and Sc_i are the hydraulic radius, Reynolds number, and Schmidt numbers, respectively, defined as

$$R_h = 2c_w c_d/2(c_w + c_d) \tag{22}$$

$$Re = 2v_g \rho R_h/\mu \tag{23}$$

$$Sc_{NO} = \mu/\rho D_{NO} \quad \text{and} \quad Sc_{NH_3} = \mu/\rho D_{NH_3} \tag{24}$$

and B, c_w, c_d, v_g, ρ, μ, and D_i are the monolith cell shape factor (2.976 for square cells), cell width, cell depth, gas velocity, gas density, gas viscosity, and molecular diffusion coefficients of NO and NH_3, respectively. The effective diffusion coefficients ($D_{e,i}$) for NO and NH_3 used in Eqs. 13, 14, and 16, are defined as

$$1/D_{e,NO} = \left(1/\epsilon^2\right)\left(1/D_{NO} + 1/D_{Kn,NO}\right) \quad \text{and}$$
$$1/D_{e,NH_3} = \left(1/\epsilon^2\right)\left(1/D_{NH_3} + 1/D_{Kn,NH_3}\right) \tag{25}$$

where ϵ is the catalyst porosity, and $D_{Kn,i}$ is the Knudsen diffusion coefficients for NO and NH_3 in circular pores. D_i and $D_{Kn,i}$ are derived from published equations and intermolecular parameters (Smith, 1981; Bird et al., 1960).

The porous catalyst model describing diffusion and reaction inside the porous ceramic was formulated using a modified finite difference formulation presented by Lin et al. (1991). The numerical solution is based on the approach developed by Spalding (1972) and Roscoe (1975) of replacing finite difference formulations of individual derivatives by a difference equation formulation of the actual ordinary differential equation (ODE). Formulation using a collapsing grid (at the pore mouth) can be applied using Cassaroti's Theorem (Hahn and Wendt, 1985). This finite difference approach gives zero truncation error for an ODE with constant coefficients, while the more traditional Taylor Series finite difference formulations do not (Hahn and Wendt, 1985). For all the calculations presented here, the pore was divided into 50 mesh intervals, with a mesh interval shrink factor of 0.85 ($h_{j+1}/h_j = 0.85$) to provide for very fine resolution at the pore mouth, where steep concentration gradients occur. At each axial step, an iterative procedure yielded the NO and NH_3 profiles inside the catalyst monolith. The first iteration yielded the NO profile for a constant NH_3 composition, for which an analytical solution is available (Levenspiel, 1972). In every case, the numerical first iteration was shown to be identical to the analytical solution, confirming the absence of any numerical errors and inaccuracies in the rather complex finite difference formulation and complicated boundary conditions. The calculated NO profile was then used to calculate an NH_3 profile, by solving Eq. 14, and the ensuing NH_3 values were inserted in the next iteration to calculate a new NO profile. Convergence usually occurred within nine iterations. Calculation of NH_3 concentrations by difference, as suggested by Beeckmann and Hegedus (1991), did not work here because, when $C_{NH3} \ll C_{NO}$, very small errors in the NO concentration resulted in negative calculated NH_3 concentrations and numerical instabilities.

Axial integration of Eqs. 17 and 18 along the monolith employs Hindmarsh's LSODE code (Hindmarsh, 1980), as does the SNCR code (described in greater detail below). Integration was terminated when the NH_3 level in the bulk stream was reduced to less than 5 ppm, because an NH_3 slip of 5 ppm was set as a practical constraint to the problem. If NH_3 in the bulk gas were allowed to fall below 1 ppm with appreciable NO values remaining, then, in this formulation, the pore iterations sometimes failed to converge.

Comparison of SCR model prediction to data

Table 2 presents 30 sets of experimental data for both the SCR-only tests (Series 1 and 2). These data were compared to the SCR model. The third column of Table 1 presents values for the reactor parameters and gas parameters used in the SCR model. These were determined *a priori*, from physical measurements of the actual catalyst used, and were not adjusted thereafter. The catalyst specific surface area S_v (m^2/m^3) was obtained from the directly measured (helium) BET internal surface area of 7.704×10^4 m^2/kg (77.04 m^2/g) and an assumed superficial density of 1×10^3 kg/m^3 (1 g/cm^3) [later verified to be 9.6×10^2 kg/m^3 (0.96 g/cm^3) from direct measurements, $= \rho_{cat}(1 - \epsilon)$]. Catalyst pore specific volumes and average pore diameters were also determined from direct measurements.

Three multivariable nonlinear regressions were performed using the integral SCR reactor data and model predictions.

Table 3. SCR Model Parameters

Parameter	Beeckman and Hegedus*	Two-Parameter Fit	Three-Parameter Fit
k_o	8.640e + 1 m/s [8.640e + 3 cm/s]	1.520e + 3 m/s [1.520e + 5 cm/s]	6.864e + 8 m/s [6.864e + 10 cm/s]
E	7.954e + 4 J/mol [1.900e + 4 cal/mol]	7.954e + 4 J/mol [1.900e + 4 cal/mol]	1.343e + 5 J/mol [3.209e + 4 cal/mol]
K_{NH_3}	1.054e + 2 m^3/mol [1.054e + 8 cm^3/mol]	3.778 m^3/mol [3.778e + 6 cm^3/mol]	3.946 m^3/mol [3.946e + 6 cm^3/mol]
Correlation coeff. (r^2)	0.935	0.942	0.952

*k_0 and E taken from Beeckman and Hegedus (1991) with K_{NH3} determined from a one-parameter fit of the data.

The nonlinear regression program XTRACTR (White, 1975) that was used is based on the Marquardt algorithm, and employs (where applicable) reparameterization to allow determination of both the pre-exponential factor and activation energy to alleviate poorly conditioned parameter response surface problems.

The first nonlinear regression calculation used the kinetic parameters for k_0 and E given by Beeckman and Hegedus (1991) and only the unknown NH_3 adsorption coefficient (K_{NH_3}) was determined. Results are shown in the upper panel of Figure 3, and in Table 3. There is excellent agreement between model predictions and the data over a very wide range of NO and NH_3 concentrations, with a correlation coefficient (r^2) of 0.935. This agreement also suggests that the intrinsic kinetic parameters of Beeckman and Hegedus (1991) are valid under the conditions examined here. Using their published values for k_0 and E, the newly derived value of the NH_3 adsorption coefficient (K_{NH_3}) is 1.054×10^2 m^3/mol (1.054×10^8 cm^3/mol). With this adsorption coefficient, the kinetics approach first-order behavior in NO when the NH_3 concentration is larger than 400 ppm. This is seldom solely the case when an NH_3 slip of 5 ppm is imposed on the outlet stream.

For a second set of nonlinear regression calculations, two kinetic parameters (k_0 and K_{NH_3}) were allowed to vary in order to attempt better fit to the data. Results led to a slightly better correlation, and the new parameter values are shown in Table 3. Finally, all three parameters, k_0, E, and K_{NH_3}, were allowed to vary, and the nonlinear regression produced revised values and a correlation coefficient increasing slightly to 0.952.

Comparison of model predictions using these parameter values and the data is shown in the lower panel of Figure 3. However, the ensuing "best fit" parameters were substantially changed, as shown in Table 3, and the improvement in correlation coefficient is not sufficiently great, in our opinion, to discard the known intrinsic values for k_0 and E available from Beeckman and Hegedus (1991). These new "best fit" values are reported here for the sake of completeness, and on the chance that unpublished additional data might exist elsewhere. These data can be better correlated over a wider range by this newly derived rate constant with the higher activation energy. Note that over the 50 K temperature range of the data presented here, we have assumed that the transport coefficients are approximately constant (see Table 1), and that any temperature dependencies are caused by temperature dependencies in the intrinsic reaction rate coefficient.

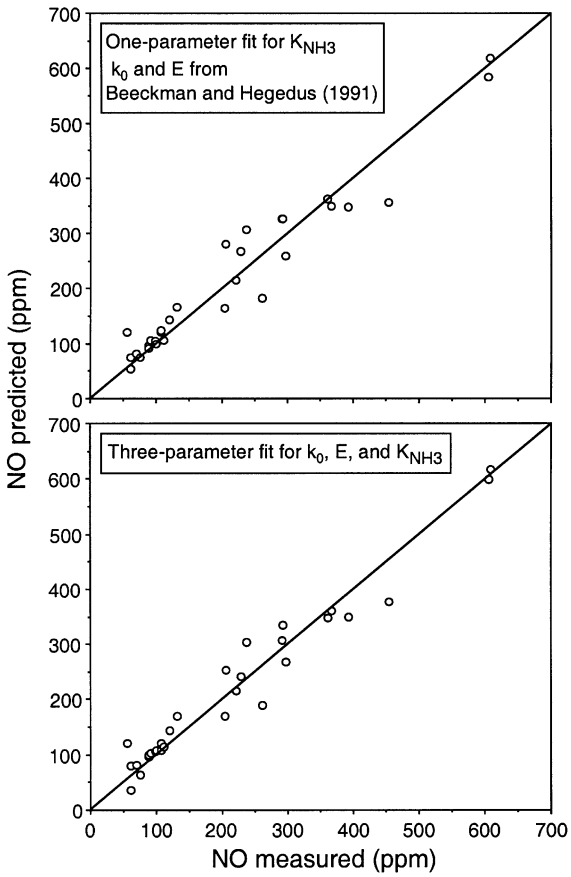

Figure 3. Predicted vs. measured NO concentrations at SCR outlet.

The top panel presents model predictions using k_0 and E taken from Beeckman and Hegedus (1991) and a one-parameter fit of data (Table 2) to determine K_{NH_3}. The bottom panel presents model predictions using a three-parameter fit of the data to determine k_0, E, and K_{NH_3}.

SNCR and Combined SNCR-SCR Models

SNCR, with NH_3 addition, involves multiple homogeneous gas-phase reactions summarized by Miller and Bowman (1989). Here, a modified Miller and Bowman mechanism involving 32 species and 112 reactions was used. The 243-reaction mechanism outlined in Appendix A of their article (Miller and Bowman, 1989) was used as a starting point with species and associated reactions eliminated for applicability to SNCR environments. Reactions involving fuel species (such as C_xH_y) were removed. The resulting reaction set included Reactions 38, 39, 55–64, 102, 103, 130–150, 152, 155, 156, 161, 163, 166, 167, 171–196, and 198–234 from Appendix A.

The SNCR process using urea addition was simulated by the thermal decomposition products of urea (Muzio et al., 1990; Braun et al., 1991; Caton and Siebers, 1989)

$$CO(NH_2)_2 \Leftrightarrow NH_3 + HNCO \qquad (26)$$

and five additional reactions involving HNCO and presented in Table 3 of Miller and Bowman (1989) were included. Finally, Reaction 197, involving $NCO + NO \Leftrightarrow N_2O + CO$, has been updated and replaced by two reactions to take into account more recent information regarding branching ratios between the products $N_2O + CO$ and $N_2 + CO_2$ (Becker et al., 1992; Kramlich and Linak, 1994). Rate constants for these two reactions were taken from a kinetic mechanism available from the Gas Research Institute (GRI-Mech 2.11, 1996).

The SNCR reactor was modeled as a plug-flow reactor with exponentially falling temperature as shown in Figure 1. Initial concentrations at the NH_3/urea injection location were given by chemical equilibrium (at that temperature) for all, except the nitrogenous, species. The numerical algorithm for the SNCR model was a CHEMKIN-based program (Kee et

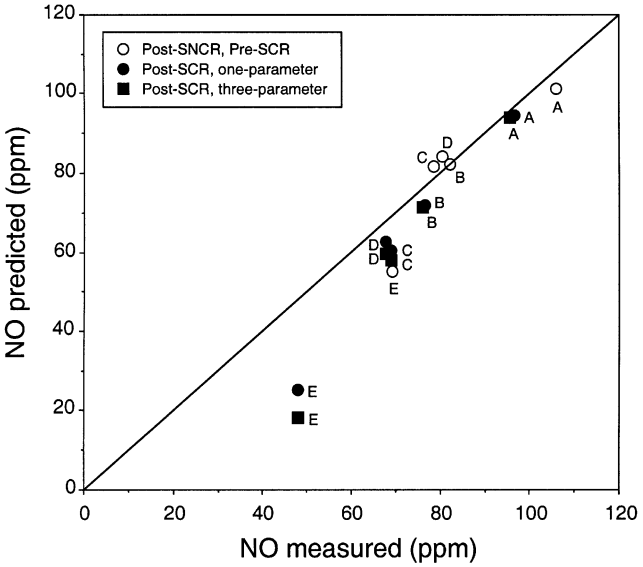

Figure 4. Predicted vs. measured NO concentrations using combined SNCR-SCR model.

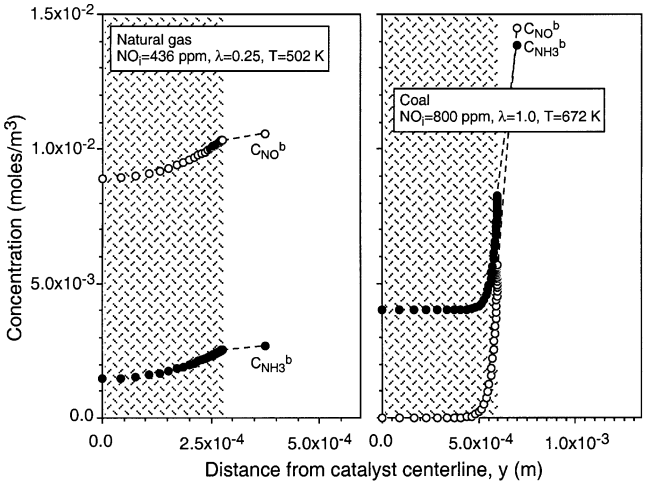

Figure 5. NO and NH_3 concentration profiles into porous catalyst for natural gas (left) and coal (right) flue-gas simulations at monolith entrance ($z = 0$ m).

Natural gas case represents actual test 2-4/9A (see Table 2).

al., 1992) allowing a seamless transition to the isothermal SCR program, with addition of NH_3 at the entrance to the SCR and either NH_3 or urea (modeled as $NH_3 + HNCO$) within the active SNCR region.

Figure 4 presents comparisons between combined model predictions (one-parameter and three-parameter, see Figure 3 and Table 3) and the data from combined SNCR-SCR tests (Test Series 3, see Table 2). Letter identifiers in Figure 4 correspond to those listed in Table 2. No additional parameters were adjusted. Agreement between NO values after the SNCR and after the SCR is very good. Some discrepancies might be expected from possible transverse variations of the NH_3/NO ratio in the duct and these could not be measured. The larger discrepancies at ~ 45 ppm NO might be due to failure to achieve steady state in the SCR under those conditions. It is noteworthy that the homogeneous detailed reaction scheme describing SNCR seems to do a very good job in predicting the NO concentration entering the SCR reactor. Figure 4 also suggests that the two kinetic parameters suggested by Beekman and Hegedus (1991), plus the newly derived NH_3 adsorption constant, are sufficient to describe the data, and that little is to be gained in subsequent work by adopting the three new parameters.

Predictions and Model Extrapolation to Coal Combustion

Table 1 shows differences in parameters for SCR as realized in the natural gas experimental data presented here (3rd column), and for SCR as applied at full-scale for NO control for coal combustion flue gases (4th column). Note specifically the differences (experimental combustor vs. full-scale coal combustor) in operating temperature (523 vs. 672 K), gas velocity [1.54 vs. 9.10 m/s (154 vs. 910 cm/s)], monolith cell wall thickness [5.5×10^{-4} vs. 1.2×10^{-3} m (0.055 vs. 0.12 cm)], and cell dimensions [3.2×10^{-3} vs. 7.4×10^{-3} m (0.32 vs. 0.74 cm)]. The higher temperature (672 K) is well within the useful range for this type of catalyst (500 to 700 K) without significant NH_3 oxidation (ICAC, 1994b). Revised monolith dimensions were taken from Rummenhohl (1999), and coal properties were those of a Wyoming Powder River Basin subbituminous coal. A factor which could not be included here is the possible effect of sulfur in the flue gas which might, but need not, interfere with catalyst performance (ICAC, 1994b). Ammonium bisulfate can be maintained below levels that cause operational problems by minimizing NH_3 slip and suppressing sulfur dioxide (SO_2) oxidation. Field testing using a high sulfur (3%) U.S. coal indicated successful performance with NH_3 slip and SO_2 oxidation less than 5 ppm and 0.75%, respectively (ICAC, 1994b). Furthermore, in the absence of additional data, it was necessary to assume that the effect of temperature on the adsorption coefficient (K_{NH_3}) was negligible compared to its effect on the NO surface reaction rate, as determined by the activation energy of Beeckman and Hegedus (1991).

Catalyst profiles

Some insight into model behavior can be obtained by comparing concentration profiles inside the catalyst for the natural gas and the coal cases. This comparison is presented in Figure 5. Note that the NO and NH_3 concentration profiles for the natural gas simulation (left panel) suggest fairly slow kinetics and complete penetration to the center of the cell wall. This is a consequence of the low (nonoptimum) SCR operating temperature (~ 523 K) which was deliberately chosen since partial reductions were desired. At the more practical coal combustion flue gas conditions (right panel), the process becomes pore diffusion controlled. This indicates the importance and necessity of constructing a fundamentally based model, which included diffusion and reaction components in order to extrapolate from the partial reduction natural gas case to the more optimum application presented by the coal

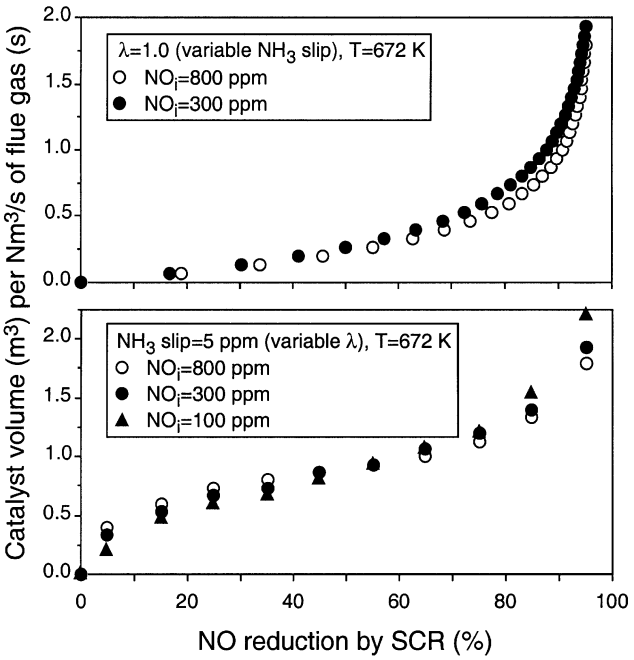

Figure 6. Predicted catalyst volume vs. NO reduction by SCR (X_{SCR}) for constant $\lambda = 1.0$, variable NH_3 slip (top), and constant NH_3 slip = 5 ppm, variable λ (bottom).

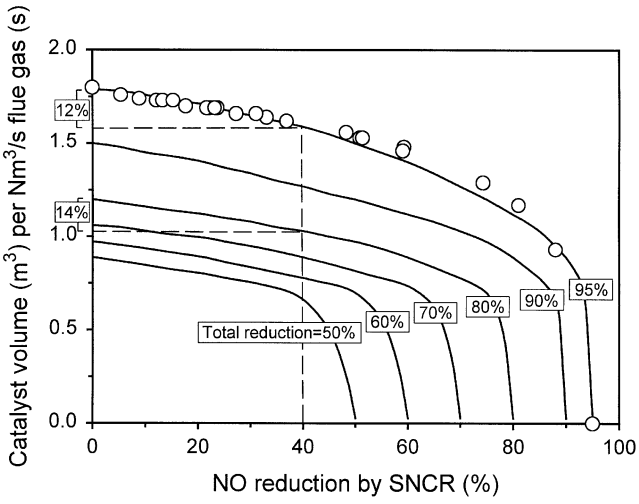

Figure 7. Predicted catalyst volume vs. NO reduction by SNCR (X_{SNCR}) for total NO reductions (X_{Total}) from 50 to 95%.

Solid curves represent the relationship between X_{SNCR}, X_{SCR}, and X_{Total} defined by Eq. 27, and the relationship between X_{SCR} and catalyst volume defined by a fourth-order polynomial fit of the model results from Figure 6 (lower panel). Open circles represent detailed model predictions for 30 cases varying λ and urea injection temperature (NO_i = 800 ppm, NH_3 slip = 5 ppm, $X_{Total} = 0.95$). These detail results are further described in Figures 8 and 9.

combustion case. A global model, with overall kinetics and no pore diffusion, would be inadequate. The steep gradients at the pore mouth for the coal combustion simulation also indicate the importance of a robust numerical model.

SCR reductions

The implementation of SCR in practice is constrained by NH_3 slip. Unless otherwise stated, we limit this slip to 5 ppm. This constraint has important implications when applied to the evaluation of relationships between required catalyst volume and NO reduction. Figure 6 shows the required catalyst volume per volumetric flow rate of flue gas vs. NO reduction for cases of constant inlet NH_3 ($\lambda = 1.0$) and variable NH_3 slip (top panel), and constant NH_3 slip (5 ppm) and variable inlet NH_3 (bottom panel). Inlet NO concentrations of 800 and 300 ppm, and 800, 300 and 100 ppm for the top and bottom panels, respectively, are examined. The nonlinear behavior is apparent especially at the high NO reduction values because of the low values of both NO and especially NH_3. Note that, for moderate NO reductions when NH_3 slip is not constrained (top panel), the required catalyst volume is very much smaller compared to the constrained case (bottom panel). However, practical applications of SCR do impose a constraint on NH_3 slip and, therefore, the bottom panel of Figure 6 describes relationships of practical importance. Again, the bottom panel relates catalyst volume and NO reduction with the NH_3 inlet adjusted so that NH_3 slip of 5 ppm occurs at each NO reduction value. The nonlinear behavior is apparent at the extremes. However, note that the full model predicts that the dependence on initial NO value from 800 to 100 ppm is slight. This observation is not obvious *a priori*, given both the complexities included in the model and the fact that the first-order kinetics should occur only for NH_3 concentrations greater than 400 ppm. However, this makes it possible to approximate predictions for a wide range of inlet NO concentrations by a single equation giving a relationship between catalyst volume and NO reduction constrained by 5 ppm NH_3 slip. Lower values of NH_3 slip would increase the required catalyst volume, but not change the general conclusions relating to the hybrid process.

The fact that SCR catalyst volume and NO reduction are only weakly dependent on inlet NO allows one to create, for the combined process, a series of plots relating required SCR catalyst volume to NO reduction by SNCR. This is because the NO reduction by SCR (X_{SCR}) is related to NO reduction by SNCR (X_{SNCR}) by

$$X_{SCR} = 1 - [(1 - X_{Total})/(1 - X_{SNCR})] \qquad (27)$$

which, together with the results in the bottom panel of Figure 6 (relating catalyst volume to X_{SCR}), leads to the results presented in Figure 7. These predictions show approximate (because of the weak dependence on inlet NO) dependence of SCR catalyst volume for various values of total (combined SNCR-SCR) reduction of NO (X_{Total}). Inspection of Figure 7 leads to an important result, namely, that catalyst volume is only modestly decreased through the application of SNCR (through urea addition). For example, if a total NO reduction of 80% is desired, and if it is assumed that SNCR can achieve 40% NO reduction, then Figure 7 indicates that this combination of SNCR-SCR would result in a 14% reduction in the

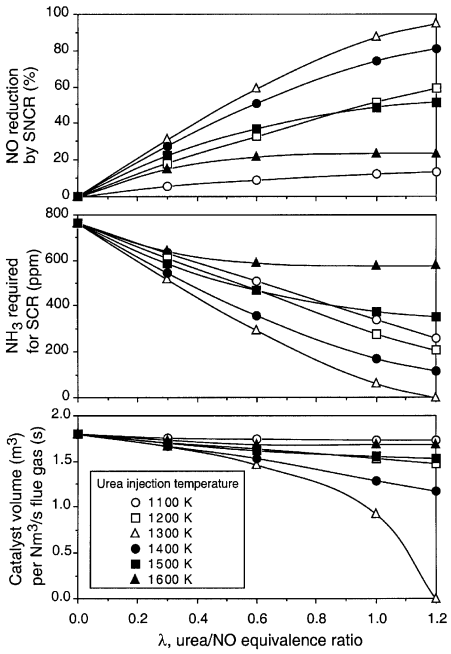

Figure 8. Predicted SNCR performance and SCR reagent (NH_3) and catalyst requirements as a function of λ and urea injection temperature.

NO_i = 800 ppm, NH_3 slip = 5 ppm, and X_{Total} = 0.95 for all cases.

required catalyst volume compared to the case with no SNCR. If the overall NO reduction desired is increased to 95%, then the catalyst volume saved with 40% NO reduction by SNCR is 12%. This is directly related to the constraint on NH_3 slip, and, because the catalyst is acting in essence, to "polish" the effluent from the SNCR zone. However, in order to estimate costs and potential cost savings by installing combined SNCR-SCR systems, one must perform detailed calculations to predict not only SCR catalyst volume requirements, but also the urea and NH_3 required. Note that under practical conditions, NH_3 slip can and does occur from the SNCR zone.

Detailed SNCR-SCR predictions

The combined SNCR-SCR model was used to yield detailed information on the relationships between catalyst volume and SNCR NO reductions (Figure 7) and the consequences associated with these relationships. Within the SNCR model, practical (or nonoptimum) reductions of NO can be achieved in two ways: by injecting the urea at a nonoptimal temperature, or by using the nonoptimal ratio of urea to NO. In Figure 8 both effects are explored. It was believed that this would provide insight into the effects of imperfect mixing (not considered by the SNCR model), since one effect of imperfect mixing might be that the average temperature and average urea/NO equivalence ratio is nonoptimum. Indeed, this is why SNCR reductions in the field are so much lower than perfectly mixed kinetic predictions and laboratory-scale experiments (Jones et al., 1995; Hunt et al., 1997).

For an initial NO concentration of 800 ppm, combined SNCR-SCR processes were investigated for 95% total NO reduction and 5 ppm NH_3 slip. Independent variables were the urea injection temperature and the urea/NO equivalence ratio. Enough NH_3 was injected after the SNCR and before the SCR to provide for 95% total NO reduction (40 ppm NO in the exhaust) with 5 ppm NH_3 slip. Calculated quantities were the NO reduction by SNCR, the amount of NH_3 that must be added between the SNCR and SCR zones in order to achieve the required overall NO reduction and NH_3 slip, and the required SCR catalyst volume.

First, these calculations yielded more precise results on the relationship between NO reduction by SNCR and the required SCR catalyst volume. The results of these more precise calculations are shown by the open circles in Figure 7 and can be compared to the approximate curve for 95% total NO reduction. Recall that the curve is approximate since it represents all of the information in Figure 6 (independent of inlet NO concentration) by a single curve. As expected, the more precise predictions fell on or close to the approximate 95% NO reduction curve. Thus, from an engineering perspective, the family of approximate curves for various total NO reductions is sufficient to calculate catalyst volume.

Second, these more precise calculations lead to the information presented on Figure 8. The independent variable is the urea/NO equivalence ratio (λ) and dependent variables are NO reduction by SNCR (X_{SNCR}), the required additional NH_3 added between the SNCR zone and the SCR reactor, and catalyst volume. Note that NH_3 can be partially converted to N_2 and NO in the SNCR zone, but not in the SCR reactor. Also, note that NO can be reduced by both NH_3 and HNCO in the SNCR zone, but only by NH_3 in the SCR reactor.

Economic analysis

Figure 8 presents the information necessary to calculate estimated costs associated with the installation and operation of combined SNCR-SCR systems. Capital costs depend most directly on the catalyst volume, while annualized costs also include the consumption of urea and NH_3 reagents. Figure 9 presents capital and annualized costs vs. λ calculated directly from the results presented in Figure 8 using the Coal Utility Environmental Cost (CUECost) model developed by Keeth et al. (1999). The CUECost model is a workbook of interrelated spreadsheets designed to produce rough-order-of-magnitude estimates of the installed capital and annualized operating costs for air-pollution control systems installed on coal-fired power plants. Model accuracy is approximately $\pm 30\%$. While the data presented in Figure 8 were calculated based on the characteristics of a Wyoming Powder River Basin (PRB) subbituminous coal burned with 20% excess air and are independent of boiler type or size, the cost data presented in Figure 9 are those for a 500 MWe utility dry-bottom boiler. Economic assumptions and consumable costs used in the CUECost calculations are listed in Table 4. As with Figure 8, the capital and annualized costs presented in Figure 9 represent conditions of varying SNCR utilization (λ and urea injection temperature) and constant initial NO concentration (800 ppm), NO reduction (95%), and NH_3 slip (5 ppm).

Figure 9 presents total SNCR-SCR capital and annualized costs (solid curves with symbols) and includes the portion of

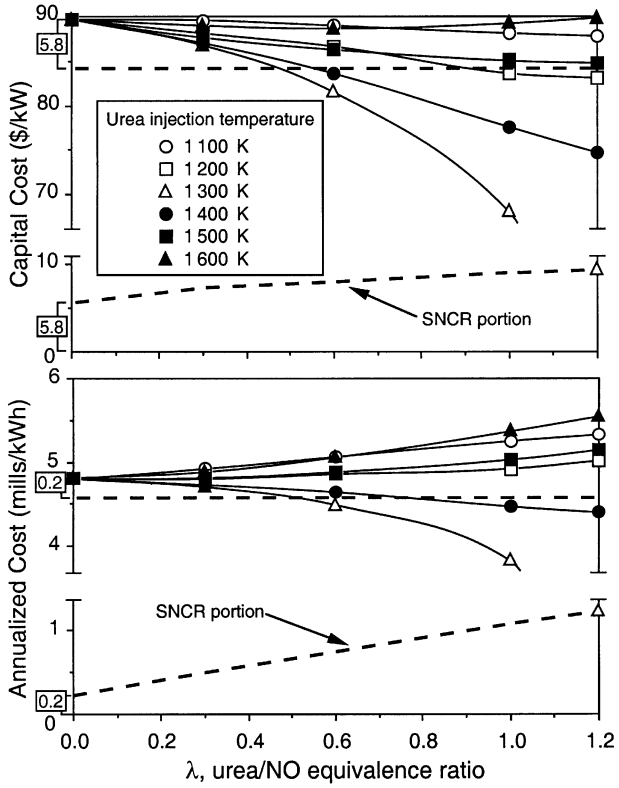

Figure 9. Predicted capital and annualized costs as a function of λ and urea injection temperature.

NO_i = 800 ppm, NH_3 slip = 5 ppm, and X_{Total} = 0.95 for all cases. Economic assumptions for the CUECost model are presented in Table 4.

those costs associated with SNCR (lower dashed lines). Note that the capital and annualized costs associated with SNCR are a relatively small fraction of the total SNCR-SCR system costs. However, as presented in Figure 9, total costs at $\lambda = 0$ include capital costs associated with SNCR, as this equipment is necessary for all other ($\lambda \neq 0$) conditions. In practice, though, a utility installing SCR alone would avoid costs associated with SNCR equipment. Therefore, comparative SCR-only capital and annualized costs have been determined from the difference of total SNCR-SCR costs and SNCR costs at $\lambda = 0$. These comparative SCR-only costs are represented by the upper horizontal dashed line on each plot. Conditions below these lines represent SNCR-SCR applications and performance yielding beneficial economics compared to SCR alone. Conditions above these lines represent uneconomical situations. In general, capital costs decrease with increasing λ, especially for scenarios where urea is injected at optimum (or near optimum) SNCR temperatures. Annualized costs do not show the same dependence on λ. Figure 9 indicates that combined SNCR-SCR systems may be economical, but only when SNCR is applied aggressively ($\lambda > 0.6$), and only when the urea reagent is introduced under optimum temperature and mixing conditions. Again, this conclusion is directly related to the constraint of 5 ppm NH_3 slip and the resulting modest reduction of SCR catalyst volume produced by the addition of SNCR (see Figure 7).

Table 4. Economic Assumption and Consumable Costs for Economic Calculations*

Description	Specification/Value
Cost year	1998
Useful life	9.4608e + 8 s (30 yr)
Levelized carrying charge	11.7%
Electric power cost	6.943e-9 $/J (0.025 $/kWh)
Urea cost	2.480e-1 $/kg (225 $/ton)
Ammonia cost	2.271e-1 $/kg (206 $/ton)
Water cost	1.1e-1 $/m^3 (0.0004 $/gal)
Catalyst cost	1.257e + 4 $/m^3 (356 $/ft^3)
Catalyst operating life	9.4608e + 7 s (3 yr)
Ash disposal cost	1.265e-2 $/kg (11.48 $/ton)
General facilities ($)	5.0% of installed cost
Eng. and home office expense ($)	10.0% of installed cost
Contingency ($)	20.0% of installed cost
Operating labor	6.94e-3 $/s [25 $/h]
Fixed O&M ($/yr)	1.5% of installed cost

*Calculations made using CUECost (Keeth et al., 1999).

Conclusions

A fundamentally based monolith model was developed for the catalytic reaction of NO and NH_3 on a porous vanadium-titanium catalyst. This model, which included pore and gas-film diffusion (molecular and Knudsen) coupled with Langmuir-Hinshelwood surface reaction kinetics, was able to predict NO reductions over a very wide range of NO and NH_3 inlet concentrations. The model required numerical solution of the pore diffusion/reaction equations and, because of the likelihood of very steep gradients at the pore mouth, used a new more accurate finite difference formulation described elsewhere.

Experimental data on the catalytic destruction of NO by NH_3 were obtained from a gas-fired 29 kW laboratory combustor, and a catalyst monolith whose physical parameters were measured *a priori*. The destruction of NO was explored over a wide range of inlet NO and NH_3 concentrations. Using kinetic parameters taken from the literature, measured porosities, and calculated transport properties, the monolith model agreed very well with the data, with adjustment of only one, previously unknown, parameter. This adjusted parameter was the NH_3 adsorption coefficient on the catalyst surface (K_{NH_3}). Together, the model and laboratory-scale data (with catalyst temperatures between 500 and 550 K) yielded a value for K_{NH_3} of 1.054×10^2 m^3/mol (1.054×10^8 cm^3/mol), with the two other kinetic parameters taken from Beeckman and Hegedus (1991). When these other two kinetic parameters (k_0, the NO destruction pre-exponential constant, and E, the NO destruction activation energy) were put into regression, the fit to the data improved only slightly. These new values of k_0 and E are given in the text, but are not proposed here as improvements over those in the literature.

This SCR model was appended to a detailed homogeneous kinetic model describing SNCR in a plug-flow reactor. Kinetic parameters for the 112 elementary reactions required were obtained from Miller and Bowman (1989), as modified

by GRI-Mech 2.11 (1996). With NH_3 as the sole reducing agent used in the 29 kW experimental combustor, this combined SNCR-SCR model was able to predict combined SNCR-SCR data before and after the catalyst monolith. No parameter in the combined model was adjusted. Agreement between data and theory was good.

When the model was extrapolated to practical coal-fired power plant conditions, it predicted significant differences in the NO profile in the porous catalyst. While the process is almost kinetically controlled at 523 K, the temperature at which the catalyst monolith was operated during the experimental effort, it is pore-diffusion-controlled at 672 K, the temperature at which typical SCR systems operate for coal-fired power plants. Hence, a fundamentally based catalytic model was shown to be essential for accurate predictions and practical extrapolations.

The model predicted that catalyst volume for a given NO reduction was insensitive to inlet NO concentration because of the (approximate) first-order dependence of the overall process on NO. This was true both for constant inlet NH_3/NO ratio ($\lambda = 1$) with variable NH_3 slip, and for constant NH_3 slip (5 ppm) with variable λ. Therefore, with the constraint of 5 ppm NH_3 slip in the catalyst exhaust, the model predicts only a modest 12% reduction of catalyst volume, gained by employing urea-based SNCR to reduce 40% of NO upstream of a SCR process with an overall NO reduction of 95%.

A coal utility environmental cost model was used to estimate capital and annualized costs of varying SNCR utilization upstream of SCR, with inlet NO concentration of 800 ppm, exit NO concentration of 40 ppm (95% reduction), and NH_3 slip of 5 ppm. This analysis indicates that only when SNCR is applied aggressively, with $\lambda > 0.6$ and SNCR reductions greater than 60%, is installation of SNCR upstream of a smaller SCR reactor economical. However, NO reductions greater than approximately 40% by SNCR are currently difficult to achieve in the field, because of mixing limitations of the nitrogen-based SNCR reagents in large ducts. Mixing limitations are not as great an issue for experimental systems, and NO reductions greater than 40% can be achieved and predicted for a bench-scale plug-flow reactor. The main practical conclusion from this work is that, in order to achieve high NO destruction (95%) with low NH_3 slip (5 ppm), there seems to be little economical advantage for the use of a hybrid SNCR-SCR process, over SCR alone. However, as the NO reduction by SNCR exceeds 60%, the hybrid process rapidly becomes economical.

Acknowledgments and Disclaimer

Portions of this work were funded through the EPA's Environmental Technology Initiative (ETI) program and conducted under EPA Purchase Orders 7D0222NATX and 8CR244NASX with J.O.L. Wendt and EPA Contract 68-D4-0005 with Acurex Environmental Corp. The authors gratefully acknowledge the contributions of D. Janek of Acurex Environmental Corp. to the experimental efforts. The research described in this article has been reviewed by the Air Pollution Prevention and Control Division, U.S. Environmental Protection Agency, and approved for publication. The contents of this article should not be construed to represent Agency policy nor does mention of trade names or commercial products constitute endorsement or recommendation for use.

Notation

A_e = monolith specific surface area, m^2/m^3
B = cell shape factor (2.976 for squares)
c_d = cell depth, m
C_i = gas concentration [i = NO or NH_3], mol/m^3
c_w = cell width, m
$D_{e,i}$ = effective diffusion coefficient [i = NO or NH_3], m^2/s
D_i = molecular diffusion coefficient [i = NO or NH_3], m^2/s
$D_{Kn,i}$ = Knudsen diffusion coefficient [i = NO or NH_3], m^2/s
E = activation energy, J/mol
F = gas flow rate, m^3/s
h_j = mesh interval, m
K_{NH_3} = NH_3 adsorption constant, m^3/mol
km_i = external mass-transfer coefficients [i = NO or NH_3], m/s
k_0 = catalyst pre-exponential factor, m/s
L = reactor axial length, m
r^2 = correlation coefficient
R = gas constant, 1.987 J/mol·K
Re = Reynolds number
R_h = hydraulic radius, m
R_i = catalyst reaction rate [i = NO or NH_3], $mol/m^2 \cdot s$
Sc_i = Schmidt number [i = NO or NH_3]
S_v = catalyst specific surface area, m^2/m^3
T = absolute temperature, K
v_g = gas velocity, m/s
V = reactor volume, m^3
W = cell wall thickness, m
X_{SNCR} = NO reduction by SNCR
X_{SCR} = NO reduction by SCR
X_{Total} = NO reduction by combined SNCR-SCR
y = catalyst wall coordinate, distance from cell wall centerline, m
z = catalyst axial coordinate, distance from catalyst inlet, m

Greek letters

ϵ = catalyst porosity
λ = NH_3 or urea/NO stoichiometric ratio
μ = gas viscosity, kg/m·s
ρ = gas density, kg/m^3
ρ_{cat} = catalyst density, kg/m^3

Subscripts and superscripts

b = bulk
i = initial
s = surface
0 = inlet

Literature Cited

Arand, J. K., L. J. Muzio, and J. G. Sotter, "Urea Reduction of NO_x in Combustion Effluents," U.S. Patent No. 4,208,386 (1980).

Becker, K. H., R. Kurtenbach, and P. Wiesen, "Investigation of the N_2O Formation in the NCO + NO Reaction by Fourier-Transform Infrared Spectroscopy," *Int. Workshop on Nitrous Oxide Emissions*, Tsukuba, Japan (1992).

Beeckman, J. A., and L. L. Hegedus, "Design of Monolith Catalysts from Power Plant NO_x Emission Control," *Ind. Eng. Chem. Res.*, **30**, 969 (1991).

Bird, R. B., W. E. Stewart, and E. N. Lightfoot, *Transport Phenomena*, Wiley, New York (1960).

Braun, A., C. Bu, U. Renz, J. Drischel, and H. J. K. Köser, "Emission of NO and N_2O from a 4 MW Fluidized Bed Combustor with NO Reduction," *Fluidized Bed Combustion: ASME 1991*, 709 (1991).

Caton, J. A., and D. L. Siebers, "Comparison of Nitric Oxide Removal by Cyanuric Acid and Ammonia," *Combust. Sci. Technol.*, **65**, 277 (1989).

Caton, J. A., and D. L. Siebers, "Effects of Hydrogen Addition on the Removal of Nitric Oxide by Cyanuric Acid," *Proc. Combust. Inst.*, **23**, 225 (1991).

Chen, S. L., J. A. Cole, M. P. Heap, J. C. Kramlich, J. M. McCarthy, and D. W. Pershing, "Advanced NO_x Reduction Processes using -NH and -CN Compounds in Conjunction with Staged Air Addition," *Proc. Combust. Inst.*, **22**, 1135 (1989).

de Soete, G. G., "Nitrous Oxide Formation and Destruction by Industrial NO Abatement Techniques, including SCR," Spring 1990 AFRC Meeting, Tucson, AZ, Institut Français du Pétrole, Report No. 37 755-10 ex., (1990a).

de Soete, G. G., "General Discussion, Conclusions, and Need for Future Work," LNETI/EPA/IFP European Workshop on the Emission of Nitrous Oxide, Lisbon, Portugal, published by Laboratorio Nacional de Engenharia e Technologia Industrial, Lisbon, Portugal (1990b).

Fujino, T., S. Kaneko, K. Suyama, and T. R. von Alten, "Experience and Consideration of SNCR-SCR Hybrid System," *EPRI/EPA 1995 Joint Symp. on Stationary Combustion NO_x Control*, Kansas City, MO (1995).

GRI-Mech 2.11, "Gas Research Institute's Combustion Mechanisms Model," Gas Res. Inst., Chicago (1996).

Groff, P. W., and B. K. Gullett, "Industrial Boiler Retrofit for NO_x Control: Combined Selective Noncatalytic Reduction and Selective Catalytic Reduction," *Environ. Prog.*, **16**, 116 (1997).

Gullett, B. K., P. W. Groff, M. L. Lin, and J. M. Chen, "NO_x Removal with Combined Selective Catalytic Reduction and Selective Noncatalytic Reduction: Pilot-Scale Test Results," *J. Air & Waste Manage. Assoc.*, **44**, 1188 (1994).

Hahn, W. A., and J. O. L. Wendt, "Integration of the Ill Conditioned System of Boundary Value ODE's for the Laminar Opposed Jet Diffusion Flame," *Stiff Differential Equations*, R. Aiken, ed., Chap. 5.2.4, Oxford University Press, New York (1985).

Hegedus, L. L., "Effects of Channel Geometry on the Performance of Catalyst Monoliths," *Am. Chem. Soc., Div. Pet. Chem.*, **18**(4), 487 (1973).

Himes, R., D. Hubbard, Z. West, and J. Stallings, "A Summary of SNCR Applications to Two Coal-Fired Wet Bottom Boilers," *EPRI/EPA 1995 Joint Symp. on Stationary Combustion NO_x Control*, Kansas City, MO (1995).

Hindmarsh, A. C., "LSODE: Livermore Solver for Ordinary Differential Equations," Lawrence Livermore National Laboratory, Tech. Report No. 3342, Livermore, CA (1980).

Hunt, T., J. L. Hebb, F. Ghoreishi, L. J. Muzio, R. A. Smith, J. Stallings, and J. H. Booher, "Using Retractable Lances to Maximize SNCR Performance," *EPRI-DOE-EPA Combined Utility Air Pollutant Control Symp.*, Washington, DC (1997).

ICAC, "White Paper: Selective Non-Catalytic Reduction (SNCR) for Controlling NO_x Emissions," Institute of Clean Air Companies, Inc., Washington, DC (1994a).

ICAC, "White Paper: Selective Catalytic Reduction (SCR) Controls to Abate NO_x Emissions," Institute of Clean Air Companies, Inc., Washington, DC (1994b).

Jones, D. G., J. Steinberger, T. Hunt, C. Barton, L. J. Muzio, J. Stallings, and R. Sherrick, "Design Optimization of SNCR DeNO_x Injection Lances," *EPRI/EPA 1995 Joint Symp. on Stationary Combustion NO_x Control*, Kansas City, MO (1995).

Kee, R. J., F. M. Rupley, and J. A. Miller, "Chemkin-II: A Fortran Chemical Kinetics Package for the Analysis of Gas Phase Chemical Kinetics," Sandia Report SAND89-8009B, Albuquerque, NM (1992).

Keeth, R., R. Blagg, C. Burklin, B. Kosmicki, D. Rhodes, and T. Waddell, "Coal Utility Environmental Cost (CUECost) Workbook User's Manual Version 1.0," EPA-600/R-99-056 (NTIS PB99-151938), U. S. EPA, Nat. Risk Manage. Res. Lab., Research Triangle Park, NC (1999).

Kramlich, J. C., and W. P. Linak, "Nitrous Oxide Behavior in the Atmosphere, and in Combustion and Industrial Systems," *Prog. Energy Combust. Sci.*, **20**, 149 (1994).

Levenspiel, O., *Chemical Reaction Engineering*, 2nd ed., Wiley, New York (1972).

Lin, W. C., J. R. Schmidt, and J. O. L. Wendt, "Modified Finite Difference Methods for Solution of Stiff Boundary Valued ODE's," AIChE Meeting, Los Angeles, CA (1991).

Linak, W. P., R. K. Srivastava, and J. O. L. Wendt, "Metal Aerosol Formation in a Laboratory Swirl Flame Incinerator," *Combust. Sci. Technol.*, **101**, 7 (1994).

Lyon, R. K., and J. A. Cole, "A Reexamination of the RapreNO_x Process," *Combust. Flame*, **82**, 435 (1990).

Lyon, R. K., "Method for the Reduction of the Concentration of NO in Combustion Effluents using Ammonia," U.S. Patent No. 3,900,544 (1975).

Meier, H., and G. Gut, "Kinetics of the Selective Catalytic Reduction of Nitric Oxide with Ammonia on a Platinum Catalyst," *Chem. Eng. Sci.*, **33**, 123 (1978).

Miller, J. A., and C. T. Bowman, "Mechanism and Modeling of Nitrogen Chemistry in Combustion," *Prog. Energy Combust. Sci.*, **15**, 287 (1989).

Muzio, L. J., T. D. Martz, T. A. Montomery, G. C. Quartucy, J. A. Cole, and J. C. Kramlich, "N_2O Formation in Selective Non-Catalytic NO_x Reduction Processes," Amer. Flame Res. Committee 1990 Fall Intl. Symp., San Francisco, CA (1990).

NESCAUM, "Status Report on NO_x Control Technologies and Cost Effectiveness for Utility Boilers," Northeast States for Coordinated Air Use Management, Boston, MA (1998).

Perry, R. A., and D. L. Siebers, "Rapid Reduction of Nitrogen Oxides in Exhaust Gas Streams, *Nature*, **324**, 657 (1986).

Perry, R. A., "NO Reduction using Sublimation of Cyanuric Acid," U.S. Patent No. 4,731,231 (1988).

Roscoe, D. F., "New Methods for the Derivation of Stable Difference Representations for Differential Equations," *J. Inst. Maths. Applics.*, **16**, 291 (1975).

Rummenhohl, V., Personal communication, Steag Aktiengesellschaft, Durham, NC (1999).

Ryan, J. V., and W. P. Linak, "On-Line Measurement of Nitrous Oxide from Combustion Sources by Automated Gas Chromatography," *5th Intl. Workshop on Nitrous Oxide Emissions*, Tsukuba, Japan (1992).

Siebers, D. L., and J. A. Caton, "Removal of Nitric Oxide from Exhaust Gas with Cyanuric Acid," *Combust. Flame*, **79**, 31 (1990).

Smith, J. M., *Chemical Engineering Kinetics*, 3rd ed., McGraw-Hill, New York (1981).

Spalding, D. B., "A Novel Finite Difference Formulation for Differential Expressions Involving both First and Second Derivatives," *Int. J. Num. Meth. Eng.*, **4**, 551 (1972).

Stamey-Hall, S., and W. Neuffer, "Alternative Control Techniques Document—NO_x Emissions from Utility Boilers," EPA-453/R-94-023 (NTIS PB94-184165), U.S. Environmental Protection Agency, Office of Air Quality Planning and Standards, Research Triangle Park, NC (1994).

Teixeira, D. P., L. J. Muzio, T. A. Montgomery, G. C. Quartucy, and T. D. Martz, "Widening the Urea Temperature Window," *1991 Joint Symp. on Stationary Combustion NO_x Control*, Vol. 3, EPA-600/R-92-093c (NTIS PB93-212868) (1992).

Urbas, J., and J. Boyle, "In Field Results of SNCR/SCR Hybrid on a Group 1 Boiler in the Ozone Transport Region," *EPRI-DOE-EPA Combined Utility Air Pollutant Control Symp.*, Washington, DC (1997).

Wallace, A. J., F. X. Gibbons, J. Boyle, J. O'Leary, D. E. Hubbard, and R. Roy, "Evaluation of Combined SNCR/SCR for NO_x Abatement on a Utility Boiler," *EPRI/EPA 1995 Joint Symp. on Stationary Combustion NO_x Control*, Kansas City, MO (1995).

White, J. W., "Parameter Estimation by Non-Linear Regressing: User Manual for XTRACTR—A Program for Non-Linear Model Building," University of Arizona, Tucson, AZ (1975).

Manuscript received June 15, 2000, and revision received May 30, 2001.